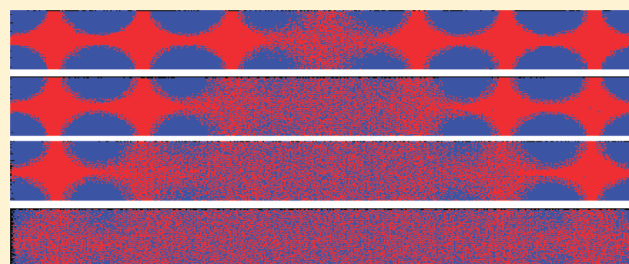


# Molecular Dynamics Study of the Response of Nanostructured Al/Ni Clad Particles System under Thermal Loading

Hong-Zhang Wu and Shi-Jin Zhao\*

Key Laboratory of Microstructures and Institute of Materials Science, Shanghai University, Shanghai 200072, China

**ABSTRACT:** Molecular dynamics simulations are used to study the exothermic alloying reactions by imposing a thermal loading on a local area of nanostructured Al/Ni clad particles. The combustion parameters, such as particles size, density, and ignition temperature, are characterized. Reducing the size of Al/Ni clad particles makes the propagation velocity of reaction front increase but lowers both the adiabatic combustion temperature and pressure of the system. However, increasing either mass density or ignition temperature makes the propagation velocity of reaction front increase and raises the adiabatic temperature and pressure as well. We estimate the propagation velocity of the chemical reaction front to range from 35.70 to 44.06 m/s.



## 1. INTRODUCTION

Nanostructured reactive materials have a wide range of applications including high temperature synthesis (SHS),<sup>1–3</sup> joining,<sup>4</sup> soldering,<sup>5</sup> etc. This class of materials can undergo rapid exothermic self-sustained reactions under external energy loading upon local ignition. Numerous studies using different energy loading, such as thermal, mechanical, shock loading, and laser, have been carried out of self-propagating formation reactions in multilayer and powder systems over the past decade.<sup>2–13</sup> Some combustion parameters, such as combustion ignition, propagation velocity, and maximum reaction temperature and so on, have been reported generally.

The ignition temperature of Al/Ni system was observed at 913 K around the melting point.<sup>6,7,14</sup> The adiabatic combustion maximum temperature can reach 1910 K.<sup>1,6,7,15</sup> As Mukasyan<sup>16</sup> suggested, the propagation mode and combustion velocity are dependent on the used experimental parameters (density, particle size, etc). However, few researches took into consideration the effect of density. It is worth noting that the femtosecond laser not only is a novel igniting source but also can ignite a local area to induce a rapid exothermic reaction. Most importantly, it reduces the igniting time to a femtosecond scale.

In this paper, we use molecular dynamics (MD) to characterize the thermal loading of the Al/Ni system and the induced chemical reactions. For this work, we focus on the effect of particle size, density, and ignition temperature on the reaction of Al/Ni clad particles and the reaction mechanism of Al/Ni composite.

## 2. MOLECULAR DYNAMICS SIMULATION

**A. Simulation Model.** The initial configurations of all simulation cells are applied three-dimensional periodic boundary conditions. Figure 1 shows such an initial structure for the Al/Ni clad

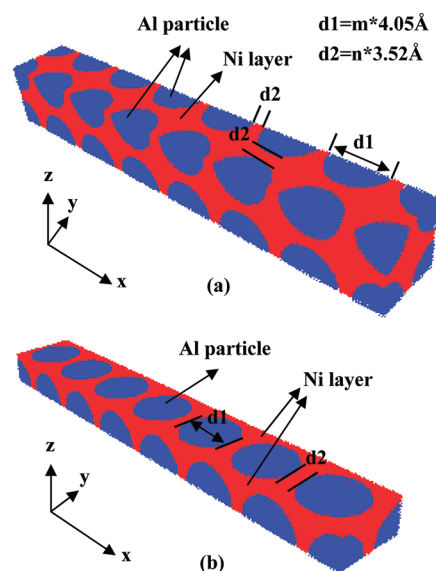


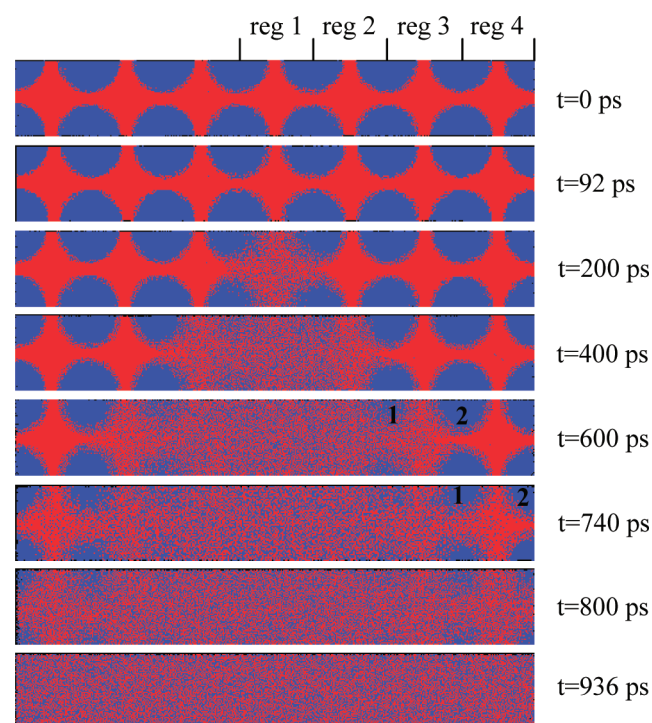
**Figure 1.** (a) Schematic of the simulation geometry.  $d_1$  and  $d_2$  represent the diameter of an Al particle and the thickness of the Ni layer.  $m$  and  $n$  is a multiple of the lattice parameters of Al and Ni, respectively. (b) Schematic of the simulation geometry (cross-sectional view).

particles. The face-centered cubic (fcc) Al nanoparticles are embedded into a fcc Ni shell in a body centered cubic structure way (Al particles clad by a thin Ni layer). The Al nanoparticle size and the thickness of Ni shell are adjusted by  $m$  and  $n$  shown in

**Received:** July 27, 2011  
**Revised:** October 18, 2011  
**Published:** October 19, 2011

**Table I. Initial Configuration of Nanostructure Al/Ni Clad Particle**

sample	$m$	$n$	Al nanoparticle diameter (nm)	thickness of Ni layer (nm)	$\rho$ ( $\text{g} \cdot \text{cm}^{-3}$ ) relaxed
sample 1	22.5	5	9.11	1.76	5.1544
sample 2	23	5	9.32	1.76	5.1135
sample 3	27.4	6	11.10	2.12	5.1383
sample 4	32	7	12.96	2.464	5.1278



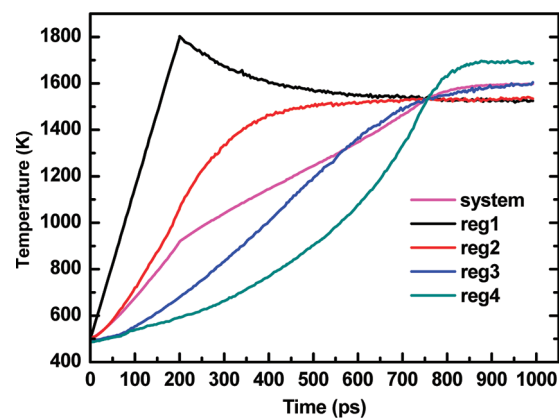
**Figure 2.** Snapshots of ignition and propagation of alloy formation for sample 2. The top frame corresponds to the time at which the sample is fully relaxed; subsequent frames (top to bottom) are shown at different times during the process of reaction. The blue and red circles represent the Ni and Al atoms, respectively. reg1, reg2, reg3, and reg4 are four regions. 1 and 2 represent the two reaction fronts.

Figure 1, noting that the choice of values of  $m$  and  $n$  is only to keep the Al/Ni ratio 1:1. All samples are a nearly equiatomic Al/Ni ratio.

To investigate the effect of nanoparticle size and mass density on an Al/Ni system, four primary samples are used in this work. The detailed sample size is listed in Table I.

The MD simulation is conducted using the LAMMPS molecular dynamics software package<sup>17</sup> provided by Sandia National Laboratories.<sup>18</sup> The results are visualized by VMD.<sup>19</sup> The Ni–Al interactions are described by an embedded atom method (EAM) potential developed by Mishin et al.<sup>20</sup> using experimental data and a large set of *ab initio* linearized augmented plane wave structural energies. This potential downloaded from NIST,<sup>21</sup> provides an accurate description of thermal expansion, diffusion and equations of state for Al, Ni and their alloys, which is of great importance for nonequilibrium atomistic simulations.

**B. Simulation Details.** To analyze and characterize the process of thermal loading and subsequent chemical reactions



**Figure 3.** Temperature as a function of time for the whole system and for the different regions in sample 2.

(both spatially), we divide the simulation model into seven equal parts. By taking into account symmetry, we only mark out reg1, reg2, reg3, and reg4 in the sample, as shown in Figure 2. The samples are relaxed  $3 \times 10^5$  steps with NPT ensemble at 500 K and 0 Pa, and all components in the stress field are very close to 0 first. Then we impose a thermal loading on only the reg1 region for 200 ps, which makes the reg1 region heat up by a heating rate of  $6.5 \times 10^{12}$  or  $5 \times 10^{12}$  K/s and increases the temperature of reg1 to a desired temperature finally. The whole process of thermal loading is continuous. Obviously, the heating rate induced by thermal loading, greatly faster than the conventional way, is similar to that induced by laser. During the process of thermal loading, the system keeps a constant volume. After thermal loading, we turn off the external heat source and describe the subsequent evolution of the system with constant energy ( $E$ ) and volume ( $V$ ) MD (NVE ensemble, where  $N$  is the number of atoms).

### 3. RESULTS AND DISCUSSION

Figure 2 shows the whole reaction process of Al and Ni for sample 2. The reaction of Al and Ni starts at the Al–Ni interface along with thermal loading on reg1. Furthermore the reaction only starts at reg1 under thermal loading. Due to the release of reaction heat, the reaction front begins propagating from reg1 to outside after the thermal loading has been turned off. The cracking of a Ni layer plays a key role in reaction of Al and Ni during the whole process. From Figure 2, the reaction of Al and Ni starts at the Al–Ni interface and makes the Ni shell gradually thinner and finally crack. There are two reaction fronts after the Ni shell cracked, which correspond to 1 and 2 in Figure 2. In reaction front 1, the Ni particles from the cracked layer and Al particles react completely. In reaction front 2, there is also a reaction of Al and Ni at their interface, which represents the main propagation direction of the reaction front. The propagation velocity of reaction front is limited by mass transfer, and the mass transfer is limited by cracking of the Ni layer. Therefore the propagation velocity is strongly dependent on the cracking of Ni layer.

Figure 3 shows the temperature profile with time at different regions in sample 2. First of all, the profile of the system temperature shows that the slope of temperature profile decreases after thermal loading, which indicates the energy release of Al/Ni reaction is smaller than the energy provide by thermal

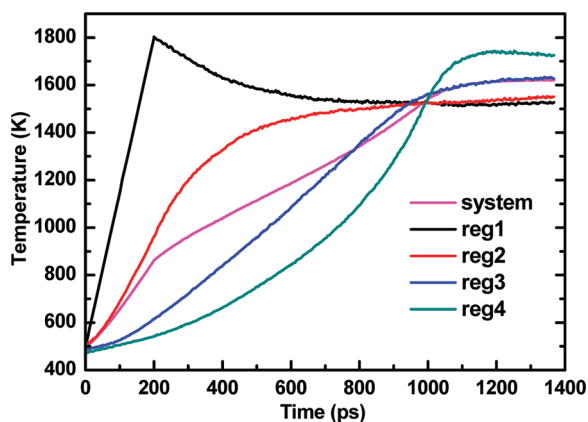


Figure 4. Temperature as a function of time for the whole system and for the different regions in sample 3.

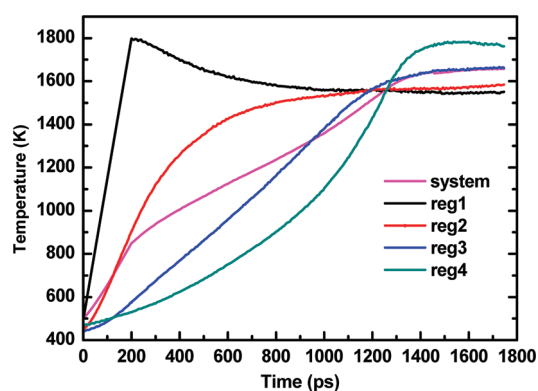


Figure 5. Temperature as a function of time for the whole system and for the different regions in sample 4.

loading. The slope of the system temperature profile increases slightly when the system temperature is above 1370 K. That means a discrete combustion, from low temperature to high temperature, exists during the process of reaction. The appearance of temperature plateau after 936 ps indicates that there is no heat release. That is to say the whole reaction is over. Second, the reg1 temperature begins to drop after thermal loading because most of the aluminum and nickel have reacted during thermal loading in this region. However, the slope of temperature decline falls slower and slower with the release of reaction heat of neighbor regions. Third, the temperature of reg2 rises steadily after thermal loading because the reaction has been ignited by thermal loading. The reactants exhausted continuously and the heat diffusion make the temperature of reg2 increase slower and slower. The slope of the temperature profile of reg3 is almost unchanged before the temperature plateau. That indicates there is an energy balance between the heat diffusion and the energy absorbed before reaction or the heat released during the reaction process.

Figures 4 and 5 show the temperature profiles with time for samples 3 and 4, respectively. The temperature histories of samples 3 and 4 display a similar result with sample 2. A comparison of temperature profiles of Figures 3, 4, and 5 shows that the highest temperatures of the system and reg4 rise with increasing the Al particle size and the thickness of Ni layer. This result is in agreement with Henz's calculation<sup>6</sup> about the coalescence of

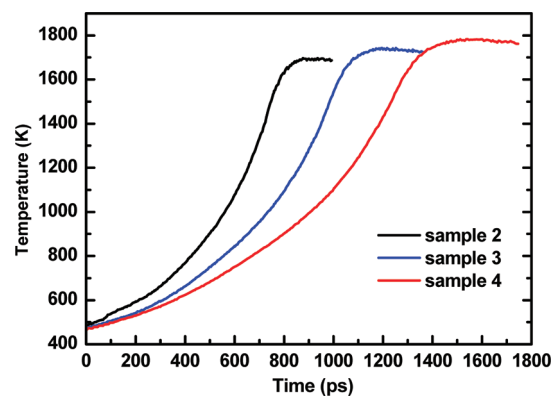


Figure 6. Temperature vs time for the reg4 region for samples 2, 3, and 4.

nanoparticles in which the temperature decreased with decreasing particles size. The experimental results<sup>4,22,23</sup> about Al/Ni multilayers also confirmed that the chemical energy stored in films was increased with increasing the thickness of Al/Ni bilayer. That was attributed to intermixing at the Al–Ni interface during layer deposition. The decrease of particle size makes the number of Al and Ni atoms increase at interface. The intermixing at the Al–Ni interface reduces the heat of reaction. Obviously, our calculation is consistent with the experimental and theoretical results.

Rather than reg1, reg2, and reg3, the temperature profile of reg4 gives us more information about the Al/Ni reaction mechanism. Figure 6 shows the comparative results of temperature profiles of reg4 for samples 2, 3, and 4. As shown in previous works,<sup>8,9,24–26</sup> the reaction starts at about the melting points of Al (933 K). Especially, Reeves observed that the unmodified Ni-clad-Al powder has a self-ignition temperature of 913 K.<sup>9</sup> Figure 6 shows the initial stage of temperature profiles for three samples increases slowly. There is a gently rising stage of temperature prior to  $\sim 913$  K for three samples which seems to indicate the ignition temperature is significantly below the melting temperature of aluminum. It is difficult to determine the ignition temperature from the temperature curve because it is relatively smooth. By observing the snapshots of combustion reaction, we find a clear sign of reaction at about 913 K for sample 2. At about 913 K, the slope of the temperature curve of sample 2 is the largest for the three samples. If the ignition starts at a similar slope for samples 2 and 3, the reaction temperature will be higher with particle size increasing. That is to say, the ignition temperature of the Al/Ni reaction increases with particle size increasing. Furthermore Puri's calculations<sup>27</sup> show that the melting temperature reaches the bulk value for 8 nm and larger-sized particles by MD. At a second stage from  $\sim 913$  to 1250 K, in agreement with Shteinberg's results,<sup>8</sup> the temperature increases quickly compared to the first stage. Shteinberg et al. attribute this stage to the reaction before the Ni layer cracked. Snapshots of the combustion reaction also confirm this point. The Ni layer does not crack at  $t = 600$  ps from Figure 2 for sample 2. The temperature of the third stage, from 1250 to about 1620, 1650, and 1680 K for samples 2, 3, and 4, respectively, goes up faster than the second stage. The contact surface of Al and Ni increases quickly along with the cracking of Ni layer. So Al particles and Ni particles react tempestuously, and the heat release increases quickly. The last stage ends at  $t = 936$ , 1252, and 1535 ps corresponding to the maximum temperature of reg4 at  $T = 1697.3$ ,

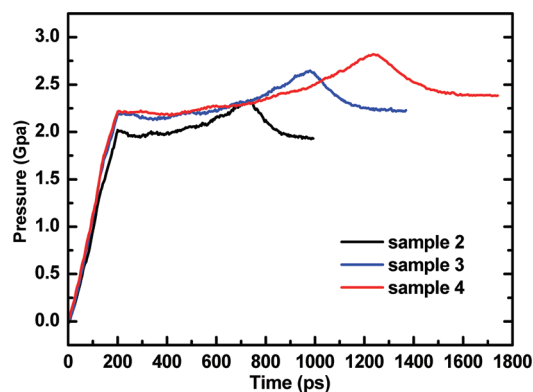


Figure 7. Pressure as a function of time for samples 2, 3, and 4.

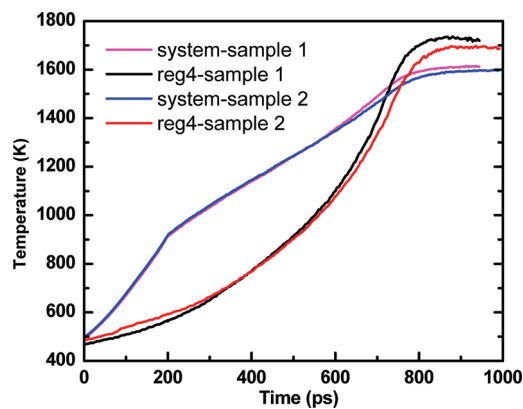


Figure 8. Temperature vs time for whole system and reg4 of samples 1 ( $\rho = 5.1544 \text{ g} \cdot \text{cm}^{-3}$ ) and 2 ( $\rho = 5.1135 \text{ g} \cdot \text{cm}^{-3}$ ).

1743.6, and 1782.9 K, respectively. The increasing rate of temperature becomes slower and slower until the temperature reaches a maximum. This stage corresponds to exhausting of reactant. The temperature of reg4 begins to fall, which is a sign that the reaction has ended. The subsequent process is a thermal equilibrium within the system. From Figure 6, a conclusion can be drawn that increasing the particle size of Al/Ni raises the adiabatic combustion temperature.

Another advantage of molecular dynamics is to trace the pressure evolution versus time. The pressure change during reaction is of importance to get the information of volume expansion, which is one of the keys to value the energetic material. Figure 7 demonstrates the pressure change of samples 2, 3, and 4. The pressure increases to 2.01, 2.19, and 2.21 GPa for samples 2, 3, and 4 after thermal loading. The maximum pressures are 2.33, 2.65, and 2.82 GPa corresponding to  $t = 740$ , 980, and 1242 ps, respectively. It is worth noting that the moment at maximum pressure does not correspond to the end of reaction. The pressure from the maximum down to an equilibrium value is another sign of the end of the reaction. The relationship between temperature and pressure is not clear. Unfortunately, there were no literature reports of the pressure change under thermal loading. From Figure 2, the outside Ni layer (in reg4) cracked completely at  $t = 740$  ps at which time the pressure begins to decrease from maximum. That is to say, there exists a local high pressure condition before the cracking of a Ni layer in an elementary cell. Thicker Ni layers suggest stronger local pressure.

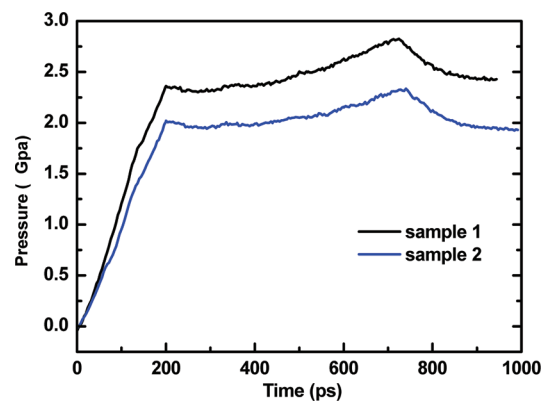


Figure 9. Pressure as a function of time for samples 1 ( $\rho = 5.1544 \text{ g} \cdot \text{cm}^{-3}$ ) and 2 ( $\rho = 5.1135 \text{ g} \cdot \text{cm}^{-3}$ ).

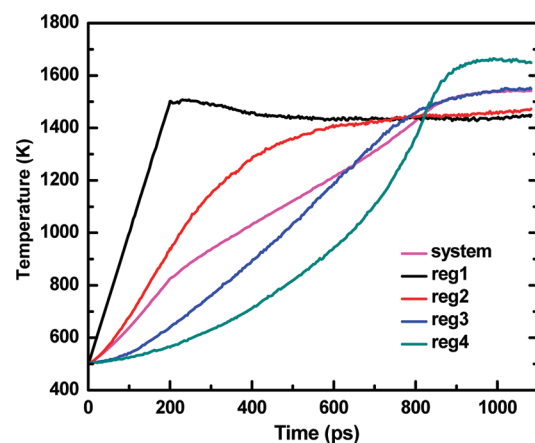


Figure 10. Temperature as a function of time for the whole system and for the different regions in sample 2.

We also examine the effect of density upon the maximum temperature and propagation velocity. From Figure 8, the maximum temperature of system and reg4 increase with increasing mass density. The stored energy is direct proportion to the density. So the released heat of reaction increases with increasing density. From Figure 9, the pressure during whole reaction process also increases with increasing mass density.

To examine the effect of ignition temperature on Al/Ni reaction, we choose another thermal loading which imposes on reg1 in sample 2 and increases the temperature of reg1 to 1500 K for 200 ps. From Figure 10, the maximum temperature reaches 1664.5 K corresponding to the time at 990 ps, and the maximum pressure reaches 2.10 GPa corresponding to the time at 810 ps. Compared to the temperature profile of sample 1 with ignition temperature at 1800 K, the maximum temperature drops by 30 K while the pressure after thermal loading and maximum pressure drop by 0.27 and 0.23 GPa, respectively.

The propagation velocity of reaction front as an important combustion parameter is to evaluate the material performance. We would use the mean propagation velocity for comparing the effect of particle size, mass density, and ignition temperature upon the reaction front. The definition of the mean propagation velocity of reaction front ( $v$ ) is as follows

$$v = \left(\frac{L}{2}\right)/t$$

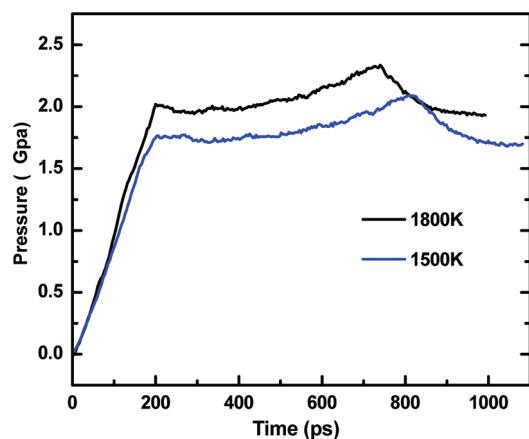


Figure 11. Pressures as a function of time for sample 2 at ignition temperatures 1500 and 1800 K.

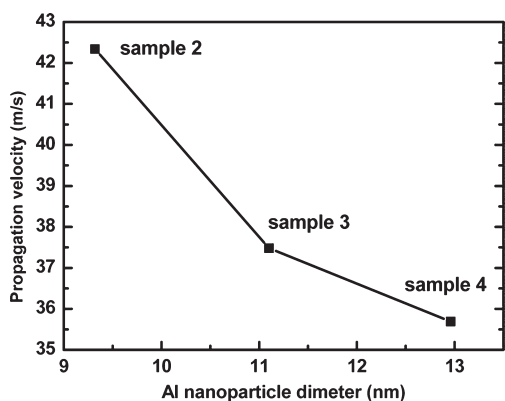


Figure 12. Propagation velocity vs Al nanoparticle diameter for samples 2, 3, and 4.

where  $L$  is a half of the sample length after relaxation and  $t$  is the time at which corresponds to the maximum temperature of reg4. The lengths after relaxation are 77.275, 79.251, 93.840, and 109.09 nm for samples 1, 2, 3, and 4.

The mean propagation velocities at ignition temperature 1800 K for samples 1, 2, 3, and 4 are 44.06, 42.34, 37.59, and 35.70 m/s, respectively. The mean propagation velocity at ignition temperature 1500 K for sample 2 is 40.00 m/s. It is well-known that the propagation velocity decreases with increasing particle size. The same trend can be seen from Figure 12. As mentioned above, cracking of the Ni layer, as an important part during whole reaction process, becomes difficult with increasing the thickness of the Ni layer. Furthermore the reactant diffusion is blocked which reduces the propagation velocity of reaction front. The mass density from 5.1544 to 5.1135 g/cm<sup>-3</sup> corresponds to the mean propagation velocity from 44.06 to 42.34 m/s for samples 1 and 2. The propagation velocity increases with increasing the mass density. Mukasyan's group<sup>16,24</sup> verified that the combustion front velocity increased with increasing density monotonically below a critical value. The ignition temperature from 1500 to 1800 K corresponds to a mean propagation velocity from 40.00 to 42.34 m/s for sample 2. The propagation velocity is faster than the reported results of the Al/Ni system. After all, the sample size in this paper is smaller than those used in experiments. As the calculations showed, the particle size has a significant impact on

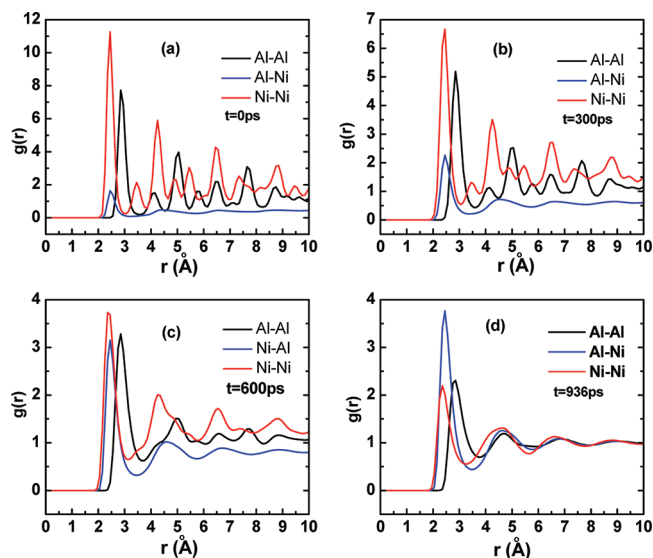


Figure 13. Comparison of radial distribution functions  $g_{\text{Al-Al}}(r)$ ,  $g_{\text{Al-Ni}}(r)$ , and  $g_{\text{Ni-Ni}}(r)$  at different times: (a)  $t = 0$  ps, (b)  $t = 300$  ps, (c)  $t = 600$  ps, (d)  $t = 936$  ps.

propagation velocity. And the temperature of thermal loading is greatly higher than the temperature obtained the conventional way. However, recent pulsed laser ignition on Al/Pt nanolaminates measured velocities ranging from 40 to 70 m/s.<sup>13</sup> These calculations are in good agreement with the previous results discussed above.

The evolution of atomic structure as the alloying reactions process is examined by comparing their radial pair distribution functions  $g(r)$ . In Figure 13, the radial pair distribution functions of  $g_{\text{Al-Al}}(r)$ ,  $g_{\text{Al-Ni}}(r)$ , and  $g_{\text{Ni-Ni}}(r)$  at different times show a transformation from heterogeneous phase of Al and Ni to homogeneous phase of NiAl. At  $t = 0$  ps, the peak intensity and peak number of  $g_{\text{Al-Ni}}(r)$  can be ignored compared to  $g_{\text{Al-Al}}(r)$  and  $g_{\text{Ni-Ni}}(r)$ . It shows that the pure Ni and Al solid phase is dominant in the system. The lattice parameters of aluminum and nickel are 0.352 and 0.405 nm, so the peak intensity of  $g_{\text{Ni-Ni}}(r)$  is the strongest. From Figure 13, the peak intensity of  $g_{\text{Al-Al}}(r)$  and  $g_{\text{Ni-Ni}}(r)$  weakens and the peak intensity of  $g_{\text{Al-Ni}}(r)$  strengthens progressively as the reaction of aluminum and nickel proceeds. When the peak intensity of  $g_{\text{Al-Al}}(r)$  and  $g_{\text{Ni-Ni}}(r)$  weakens, that means the fcc Al and Ni decreases steadily. When the peak intensity of  $g_{\text{Al-Ni}}(r)$  strengthens that means the disorder NiAl phase increases. The change of peak numbers of  $g_{\text{Al-Al}}(r)$ ,  $g_{\text{Al-Ni}}(r)$ , and  $g_{\text{Ni-Ni}}(r)$  also indicates the reactants, solid Al and Ni phase, decrease and the products, NiAl phase, increase. Especially in Figure 13c, the second peaks of  $g_{\text{Al-Al}}(r)$  and  $g_{\text{Ni-Ni}}(r)$  almost disappeared. That indicates the fcc Al and Ni become disordered for the whole system. At  $t = 936$  ps corresponding to the end of the reaction, the peak intensity of  $g_{\text{Al-Ni}}(r)$  reaches the maximum, the peak intensities of  $g_{\text{Al-Al}}(r)$  and  $g_{\text{Ni-Ni}}(r)$  are almost equal, and the curves of  $g_{\text{Al-Al}}(r)$  and  $g_{\text{Ni-Ni}}(r)$  become smooth. That indicates the system has transferred into the homogeneous NiAl phase.

#### 4. CONCLUSION

We have presented MD simulations of the alloying reaction process of nanostructured Al/Ni clad particles. The calculations

indicate that the properties of nanostructured Al/Ni clad particles depend strongly on their nanostructures and combustion parameters such as particle size and mass density. With the particle size increasing, both the adiabatic temperature and pressure of system rise but the propagation velocity of the reaction front decreases. However, when either mass density or ignition temperature increase, the adiabatic combustion temperature, the pressure of the system, and the propagation velocity of the reaction front increase. The cracking of the nickel layer, governing the contact surface and mass diffusion of aluminums and nickels, plays a key role in the propagation process of Al/Ni clad particles.

## AUTHOR INFORMATION

### Corresponding Author

\*E-mail: shijin.zhao@shu.edu.cn.

## ACKNOWLEDGMENT

This work is financially supported by the Key Project of Innovation Program of Shanghai Municipal Education Commission (Grant No. 10ZZ62), the National Natural Science Foundation of China (Grant No. 50931003), Shanghai Committee of Science and Technology (Grants No. 09520500100 and 10PJ1403900), and Shu Guang Project (Grant No. 09SG36). High performance computing resources are provided by the Ziqiang Supercomputer Center at Shanghai University.

## REFERENCES

- (1) Dyer, T. S.; Munir, Z. A.; Ruth, V. The Combustion Synthesis of Multilayer NiAl Systems. *Scr. Metall.* **1994**, *30*, 1281.
- (2) Phung, X.; Groza, J.; Stach, E. A.; Williams, L. N.; Ritchey, S. B. Adiabatic Temperature of Combustion Synthesis of Al-Ni Systems. *Mater. Sci. Eng., A* **2003**, *359*, 261.
- (3) Li, H. P. Influence of Ignition Parameters on Micropyretic Synthesis of NiAl Compound. *Mater. Sci. Eng., A* **2005**, *404*, 146.
- (4) Wang, J.; Besnoin, E.; Duckham, A.; Spey, S. J.; Reiss, M. E.; Knio, O. M.; Weihs, T. P. Joining of Stainless-steel Specimens with Nanostructured Al/Ni Foils. *J. Appl. Phys.* **2004**, *95*, 248.
- (5) Wang, J.; Besnoin, E.; Duckham, A.; Spey, S. J.; Reiss, M. E.; Knio, O. M.; Powers, M.; Whitener, M.; Weihs, T. P. Room-temperature soldering with nanostructured foils. Pulsed Laser Ignition of Reactive Multilayer Films. *Appl. Phys. Lett.* **2003**, *83*, 3987.
- (6) Henz, B. J.; Hawa, T.; Zachariah, M. Molecular Dynamics Simulation of the Energetic Reaction Between Ni and Al Nanoparticles. *J. Appl. Phys.* **2009**, *105*, 12430.
- (7) White, J. D. E.; Reeves, R. V.; Son, S. F.; Mukasyan, A. S. Thermal Explosion in Al-Ni System: Influence of Mechanical Activation. *J. Phys. Chem. A* **2009**, *113*, 13541.
- (8) Shteinberg, A. S.; Lin, Y.; Son, S. F.; Mukasyan, A. S. Kinetics of High Temperature Reaction in Ni-Al System: Influence of Mechanical Activation. *J. Phys. Chem. A* **2010**, *114*, 6111.
- (9) Reeves, R. V.; Mukasyan, A. S.; Son, S. F. Thermal and Impact Reaction Initiation in Ni/Al Heterogeneous Reactive Systems. *J. Phys. Chem. C* **2010**, *114*, 14772.
- (10) Zhao, S.; Germann, T. C.; Strachan, A. Atomistic Simulations of Shock-induced Alloying Reactions in Ni/Al Nanolaminates. *J. Chem. Phys.* **2006**, *125*, 164707.
- (11) Zhao, S.; Germann, T. C.; Strachan, A. Molecular Dynamics Simulation of Dynamical Response of Perfect and Porous Ni/Al Nanolaminates Under Shock Loading. *Phys. Rev. B* **2007**, *76*, 014103.
- (12) Zhao, S.; Germann, T. C.; Strachan, A. Melting and Alloying of Ni/Al Nanolaminates Induced by Shock Loading: A Molecular Dynamics Simulation Study. *Phys. Rev. B* **2007**, *76*, 104105.
- (13) Picard, Y. N.; Adams, D. P.; Palmer, J. A.; Yalisove, S. M. Pulsed Laser Ignition of Reactive Multilayer Films. *Appl. Phys. Lett.* **2006**, *88*, 144102.
- (14) Mukasyan, A. S.; White, J. D. E.; Kovalev, D.; Kochetov, N.; Ponomarev, V.; Son, S. F. Dynamics of Phase Transformation During Thermal Explosion in the Al-Ni System: Influence of Mechanical Activation. *Phys. B (Amsterdam, Neth.)* **2010**, *405*, 778.
- (15) Mann, A. B.; Gavens, A. J.; Reiss, M. E.; Heerden, D. V.; Bao, G.; Weihs, T. P. Modeling and Characterizing the Propagation Velocity of Exothermic Reactions in Multilayer Foils. *J. Appl. Phys.* **1997**, *82*, 1178.
- (16) Mukasyan, A. S.; Rogachev, A. S. Discrete Reaction Waves: Gasless Combustion of Solid Powder Mixtures. *Prog. Energy Combust. Sci.* **2008**, *34*, 377.
- (17) Plimpton, S. J. Fast Parallel Algorithms for Short-Range Molecular Dynamics. *J. Comput. Phys.* **1995**, *117*, 1.
- (18) LAMMPS Molecular Dynamics Simulator. <http://lammps.sandia.gov> (accessed Oct 21, 2010).
- (19) Humphrey, W.; Dalke, A.; Schulten, K. VMD - Visual Molecular Dynamics. *J. Mol. Graphics* **1996**, *14*, 33.
- (20) Mishin, Y.; Mehl, M. J.; Papaconstantopoulos, D. A. Evaluation of Diffusion Mechanisms in NiAl by Embedded-atom and First-principles Calculations. *Phys. Rev. B* **2002**, *65*, 224114.
- (21) NIST Interatomic Potentials Repository: <http://www.ctcms.nist.gov/potentials>
- (22) Gavens, A. J.; Heerden, D. V.; Mann, A. B.; Reiss, M. E.; Weihs, T. P. Effect of Intermixing on Self-propagating Exothermic Reactions in Al/Ni Nanolaminate Foils. *J. Appl. Phys.* **2000**, *87*, 1255.
- (23) Morris, C. J.; Marya, B.; Zakar, E.; Barron, S.; Fritz, G.; Knio, O.; Weihs, T. P.; Hodgkin, R.; Wilkins, P.; May, C. Rapid Initiation of Reactions in Al/Ni Multilayers With Nanoscale Layering. *J. Phys. Chem. Solids* **2010**, *71*, 84.
- (24) Mukasyan, A. S.; Lau, C.; Varma, A. Gasless Combustion of Aluminum Particles Clad Nickel. *Combust. Sci. Technol.* **2001**, *170*, 67.
- (25) Shafirovich, E.; Mukasyan, A. S.; Thiers, L.; Varma, A.; Legrand, B.; Chauveau, C. Ignition and Combustion of Al Particles Clad by Ni. *Combust. Sci. Technol.* **2002**, *174*, 127.
- (26) Thiers, L.; Mukasyan, A. S.; Varma, A. Thermal Explosion in Ni-Al System: Influence of Reaction Medium Microstructure. *Combust. Flame* **2002**, *131*, 198.
- (27) Puri, P.; Yang, V. Effect of Particle Size on Melting of Aluminum at Nano Scales. *J. Phys. Chem. C* **2007**, *111*, 11776.